Journal of the National Academy of Forensic Engineers®

http://www.nafe.org

ISSN: 2379-3252

DOI: 10.51501/jotnafe.v39i2

Vol. 39 No. 2 December 2022

Failure Analysis of Cylinder Used In a Car Flipper Device

By Faisal Khan, PEng (NAFE 1026M) and Altaf Gafoor, PEng (NAFE 1185A)

Abstract

A car flipping device is a special effects aid used to flip cars in the production of movies and television shows. The device uses a pivoting arm that moves under the stroke of a cylinder powered by compressed nitrogen. In a trial run of the device, the cylinder's piston broke through the cylinder cap. A kinematic analysis developed a parametric mathematical model of the motion of the cylinder arm and piston, which formed the basis for a finite difference analysis to determine the speed of the cylinder's piston at the end of its stroke. Metallurgical testing was conducted on the broken cylinder to determine the stress-strain characteristics, impact resistance, and Scanning Electron Microscopy (SEM) used to examine the fracture surface. The analysis determined that the kinetic energy of the piston was adequate to cause yielding of the cylinder but not rupture. Continued usage degraded the impact resistance available until rupture occurred.

Keywords

Cylinder cap, kinematics, finite difference, fracture, impact energy, metallurgical analysis, numerical methods, pneumatic piston travel speed, forensic engineering

Introduction and Background

The production of movies and television shows often use practical special effects to enhance story telling. One such effect involves the flipping of cars using proprietary devices typically fabricated by visual effects studios. The subject of this paper is the methodology used to analyze the failure of such a device.

Figure 1 shows the general construction of the car flipper. As illustrated, the device has a steel arm that is free to rotate in the vertical plane about a hinge fixed to its base. The rotation of the car flipper's arm is controlled by a cylinder and piston that is energized using compressed nitrogen fed from an actuator. As the actuator pressure is released into the cylinder, the piston and rod extend, which causes the car flipper arm to rotate while ejecting load on the arm.

The car flipper was being tested to confirm the desired car flipping effect could be achieved. The test methodology placed the device under loading from a prop car and was fed by a compressed gas actuator. Three tests in total were conducted: the first at 1,500 psi (10.3 MPa) actuator pressure and the second and third at 3,000 psi (20.6 MPa). During the third test, the piston and rod broke through the end cap of the cylinder, maintaining sufficient velocity to remain a projectile for approximately 118.5 feet (36.1 m).

Figure 2 is a photograph of the car flipper after failure showing the location of the ruptured end cap, and **Figure 3** provides a closer view of the rupture. **Figure 4** and

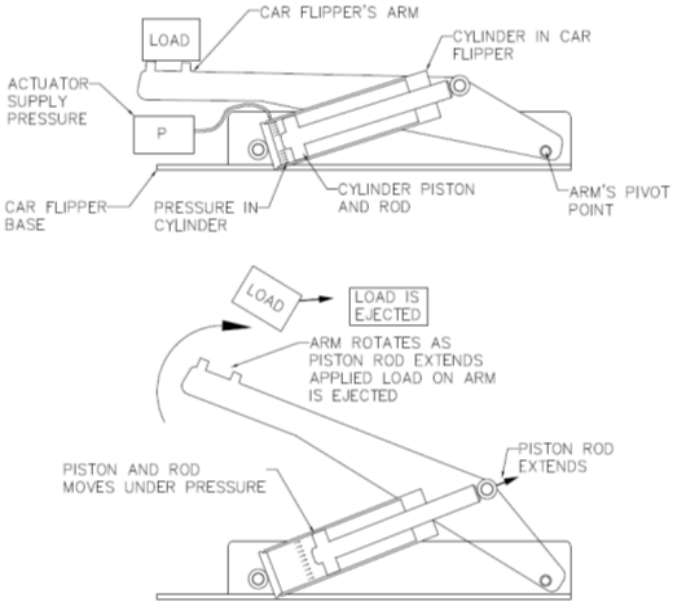

Figure 1
General construction and operation of car flipper.

Faisal Khan, PEng, 505 University Ave., 19th Fl., Toronto, ON M7A 1T7, (416) 518-7597, Faisal.Khan2@ontario.ca

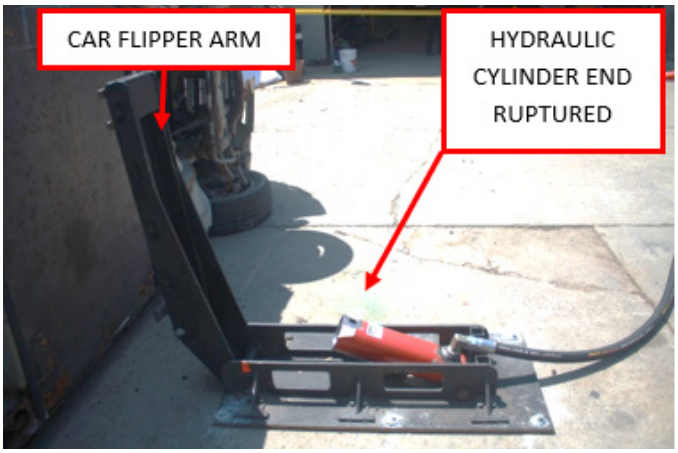

Figure 2
Close of car flipper after failure.

Figure 3
Cylinder end where cap was severed.

Figure 5 show the piston head and piston rod after the failure. As shown, the piston head did not show any significant deformation, and the piston rod was generally straight.

The design of the cylinder did not have a damping mechanism to attenuate the impact of the piston head and piston rod. The kinetic energy of the piston head and piston rod was absorbed by impact with the cylinder end cap. The hypothesis tested in this investigation was whether the piston and rod were moving with sufficient velocity such that their kinetic energy was adequate to result in a rupture of the cylinder as shown in **Figure 6**. The piston rod also

Figure 4
Inside of piston head after incident.

Figure 5
Piston rod after incident.

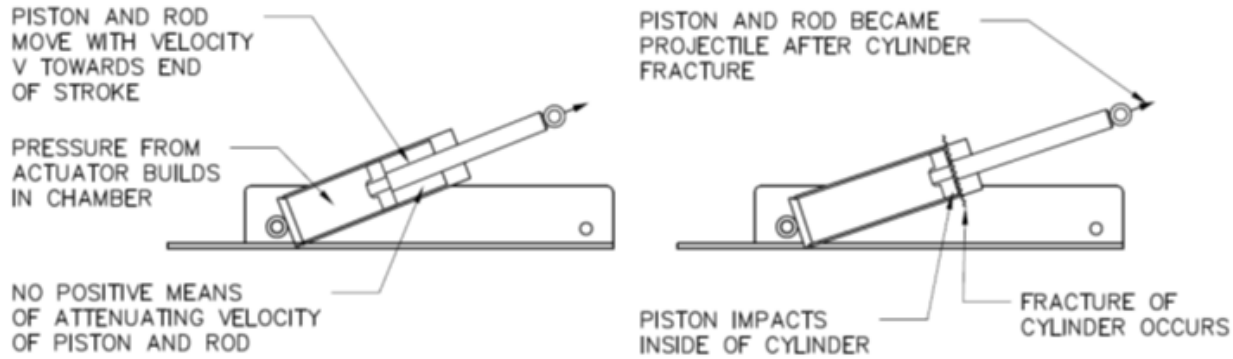

Figure 6
Impact of piston and rod on cylinder end cap. (Note: There was no positive connection — just a C-type clamp around the pin. The pin broke through the frame at its point of supports.)

broke the connection where it was secured to the car flipper's arm.

To evaluate the veracity of the hypotheses, the investigation was broken down into five components as follows:

- Component 1 utilized kinematic principles to formulate a mathematical model of the car flipper's movement.
- Component 2 derived the forces acting on the piston.
- Component 3 applied the finite difference method to estimate the velocity of the piston as it progressed through its stroke.
- Component 4 was metallurgical testing, which provided material properties and identified features of interest on the fracture surface using SEM in addition to estimating the energy required for yielding and rupture of the cylinder.
- Component 5 reviewed the manufacturer's specifications for the cylinder to ascertain the general applicability of the cylinder in the car flipper application.

Mathematical Model of Car Flipper's Movement

The first component of the investigation analyzed the spatial relationship between the movement of the car flipper's arm, the piston, and the car to be flipped with respect to fixed reference points on the car flipper. **Figure 7** shows the general arrangement and variables used to establish these relationships.

The car flipper in its application fits the definition of a mechanism[1] with points and A and C identified as the fixed reference points. The distances AC, CB, and BD (a_3) are constant, whereas the distance AB varies as the piston undergoes a displacement x_i. Points E and O are reference points that are necessary to account for the rotation of the car in response to the action of the car flipper's arm. The distances CO (a_4) and OE (a_1) are also constants. The net torque resulting from the application of the car flipper's arm pushing on the chassis of the car and resisted by the weight of the car induces an angular acceleration that contributes to the flipping of the car.

The effect of angular acceleration and angular momentum is beyond the scope of this analysis. Due to the rotational inertia gained from the car flipper, the resistance induced on the car flipper arm would decrease. Hence, the analysis conducted would produce a lower bounds estimate of the speed of the piston due to the increase in resistance to piston motion.

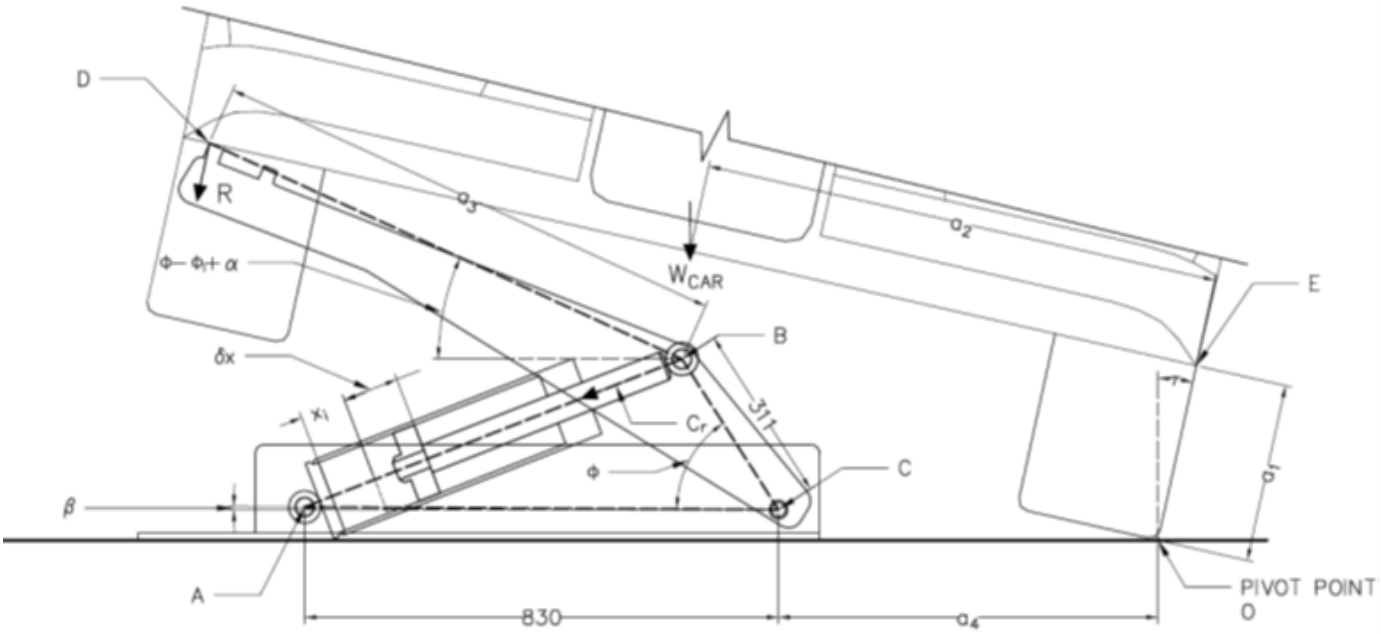

Figure 7
Geometry of car flipper adopted for mathematical model (all unis in millimeters).

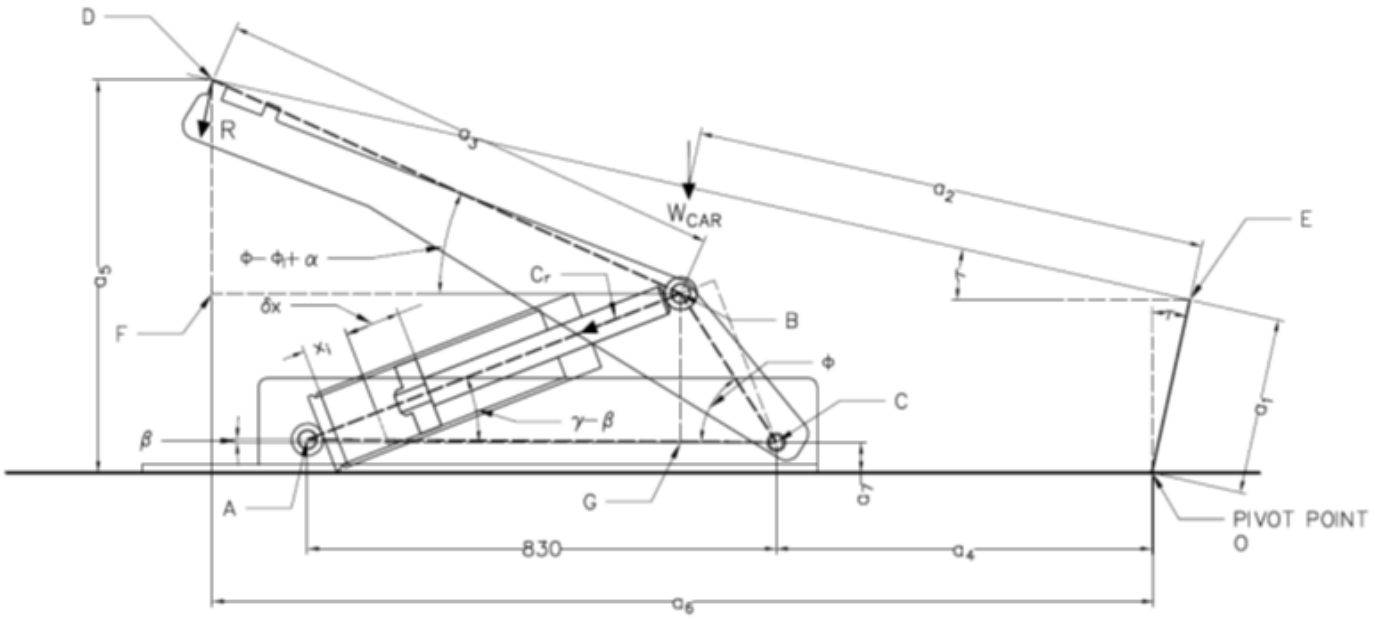

Figure 8
Identification of variables used to describe motion of car flipper's arm.

$$\tau = arcos\left(\frac{a_1}{S}\right) - U \qquad \text{EQ. 1}$$

Where,

$$S = \sqrt{a_5^2 + a_6^2}$$

$$U = \arctan\frac{a_6}{a_5}$$

$$a_5 = a_3 \sin(\emptyset - \emptyset_i + \alpha) + BC\sin(\emptyset + \beta) + a_7$$

$$a_6 = a_3 \cos(\emptyset - \emptyset_i + \alpha) + BC\cos(\emptyset + \beta) + a_4$$

$$\gamma = arcsin\left[\frac{BC}{AB_{initial} + \delta x}\sin\emptyset\right] \qquad \text{EQ. 2}$$

Where,

$AB_{initial}$ – initial length of arm AB

BC – length between points B and C, remains constant throughout event

φ – general inclination of arm CB with respect to horizontal

γ – angle BAC

EQ. 3

$$\phi = arcos\left(\frac{AC^2 + CB^2 - (AB_{initial} + \delta x)^2}{2(AC)(CB)}\right)$$

Figure 8 shows the variables used to describe the motion of the car flipper's arm as the piston extends. From this figure, the following key relationships are derived:

$$R = \frac{(a_2\cos\tau - a_1\sin\tau)}{(a_5\sin\tau + a_6\cos\tau)}W \qquad \text{EQ. 4}$$

Figure 8 also shows the reaction (R) due to the weight of the car (W), acting on the car flipper's arm. This relationship was determined to be:

EQ. 5

$$C_r = \frac{R_V[a_3\cos(\phi - \phi_i + \alpha) + BC\cos(\phi + \beta)] + R_H[a_3\sin(\phi - \phi_i + \alpha) + BC\sin(\phi + \beta)]}{830\sin(\gamma - \beta)}$$

The reaction (R) provides resistance to the motion of the piston C_r. This relationship was determined to be:

Where,

$$R_H = R\sin\tau$$

$$R_V = R\cos\tau$$

Determination of Forces on Piston

Figure 9 shows the position of the piston as it transitions from a general position x to x+δx. In **Figure 9(a)**, the piston is at a linear displacement x from its initial position. At this position, the piston is acted upon by the following pressures and forces, resulting in a velocity v_x and acceleration a_x:

- Pressure in supply line $P_{ch,x}$

- Pressure of air in cylinder $P_{cp,x}$
- Resistance on piston rod caused by car's weight $C_{r,x}$
- Air resistance to the motion of the cylinder $P_{a,x}$. (Note: This is due to the air resistance from the motion of the piston. The term $P_{cp,x}$ is due to the pressure of the air being compressed in the cylinder by its motion. The analysis is isothermal.)
- Weight component of piston's weight mg sin $(\gamma-\beta)_x$

The resulting acceleration at the general position, x, in **Figure 9(a)** is given by:

EQ. 6

$$a_x = \frac{(P_{ch,x} - P_{cp,x} - P_{a,x})A - C_{r,x} - mg\sin(\gamma-\beta)_x}{m}$$

Similarly, the resulting acceleration at the position x+δx, in **Figure 9(b)** is given by:

EQ. 7

$$a_{x+\delta x} = \frac{(P_{ch,x+\delta x} - P_{cp,x+\delta x} - P_{a,x+\delta x})A - C_{r,x+\delta x} - mg\sin(\gamma-\beta)_{x+\delta x}}{m}$$

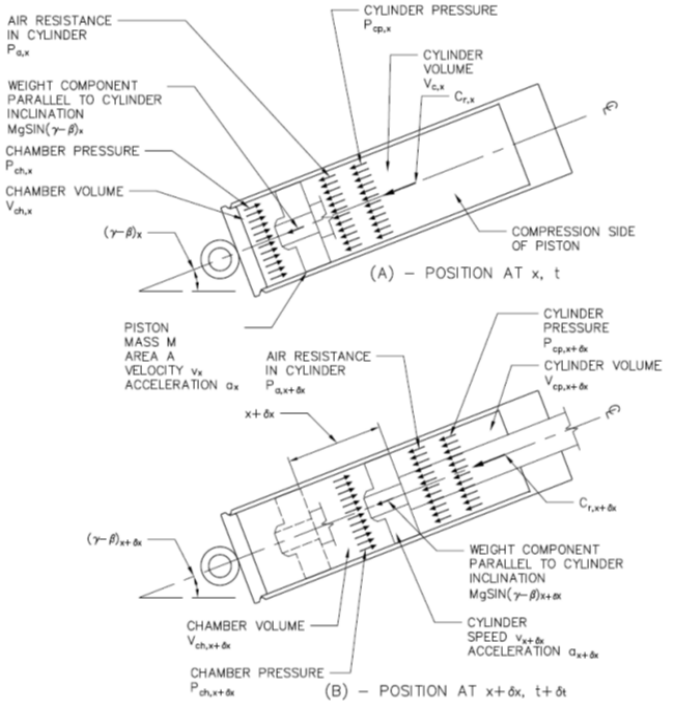

Figure 9
Forces on piston as it moves from x to x +δx.

Equations 6 and 7 provide estimates of the acceleration across a small distance δx that occurs over a small time step δt. If the time step δt is sufficiently small, then the distance step δx will also be small and:

$$\lim_{\partial x \to 0} a_{x+\partial x} \to a_x$$

Therefore, discretizing the movement of the piston in this manner allows for the application of linear equations of motion across each time and distance step. The change in velocity across each time step can be approximated using equations of motion under constant acceleration for the given step, giving: EQ. 8

$$\partial v_x = \left[\frac{(P_{ch,x} - P_{cp,x} - P_{a,x})A - C_{r,x} - mg\sin(\gamma-\beta)_x}{m}\right]\partial t$$

The conditions at t=0 and x=0 are known. Thus, Equation 8 can be applied at the initial conditions to determine the change in velocity over the time step δt. At the end of this time step, the velocity is known, and the distance moved by the piston δx can also be calculated. In this manner, the problem is spatially and temporally discretized, allowing for the continuous application of Equation 8 to evaluate the velocity and distance at further time steps.

The pressure from the actuator is released into the expansion side of the cylinder (supply chamber), which is at atmospheric pressure. The difference in pressure between the nitrogen supply and the supply chamber pressure results in a flow of mass from the actuator to the supply chamber. **Figure 10** shows the general arrangement of the actuator pressure feeding into the supply chamber. The complete isothermal equation for steady flow[2] was adopted for each time step to approximate the mass flow of gas between the supply pressure and the chamber pressure. This equation is given as:

EQ. 9

$$w^2 = \left[\frac{\rho_s A^2}{\left(\frac{fl}{D} + 2ln\left(\frac{P_s}{P_{ch}}\right)\right)}\right]\left[\frac{P_s^2 - P_{ch}^2}{P_s}\right]$$

Where,

w - mass flow rate in kilograms per second per (kg/s)

ρ_s - density of nitrogen at supply in kilograms per cubic meter (kg/m³)

P_s - absolute supply pressure in pascals (N/m²)

P_{ch} - absolute chamber pressure in pascals (N/m²)

L - length of supply line in meters (m)

A - area of supply line in square meters (m²)

D - diameter of supply line in meters (m)

f - friction factor, dimensionless

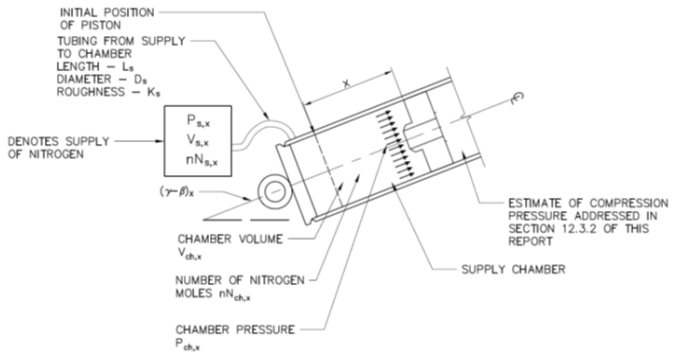

Figure 10
Supply pressure and chamber pressure.

The friction factor was calculated using the Colebroke-White equation[3] and requires the calculation of the Reynold's Number. Equation 11 requires estimates of the friction factor, which is also a function of the flow-rate. Therefore the calculation of the mass flow rate cannot be done independently of the friction factor or Reynold's Number. This problem was solved using an iteration in which a trial friction factor was assumed and the mass flow rate calculated. Based on this trial flow rate, the flow velocity and Reynold's Number was re-calculated, and using the Newton-Raphson method[4], the friction factor was calculated using the Colebrole-White equation. The mass flow rate was recalculated. If the difference between this calculated value and the initial value was outside the range +/- 0.00001, the entire iteration was repeated. This methodology was programmed using Visual Basic in Microsoft Excel.

The behavior of nitrogen approximates to an ideal gas[5] in the range of pressures and temperature (up to 3,000 psi and 305 kelvin) under consideration in this analysis. Applying the ideal gas equation, the number of moles of nitrogen entering the supply chamber was calculated as shown in Equation 10.

EQ. 10

$$\delta nN = \frac{w\delta t}{mMn}$$

Where,

δnN - change in the number of moles of nitrogen

w - mass flow rate (kg/s)

mMn - molecular mass of nitrogen (kg/moles)

The volume of the supply chamber increases as the piston moves, and the change in volume (δV) can be calculated based on the distance moved by the piston for a given time step. The volume of the nitrogen in the supply actuator does not change. Therefore, there will be a reduction of pressure in the supply actuator because there is a loss of nitrogen mass. Equations 11 and 12 estimate the pressure in supply chamber and nitrogen supply actuator at the end of each time step.

EQ. 11

$$P_{ch,x+\delta x} = \frac{(nN_{ch,x} + \delta nN)RT}{V_{ch,x} + \delta V}$$

EQ. 12

$$P_{s,x+\delta x} = \frac{(nN_{s,x} - \delta nN)RT}{V_s}$$

Where,

$P_{s,x+\delta x}$ - Pressure in nitrogen supply and end of time step (Pa)

$nN_{s,x}$ - Number of moles of nitrogen in supply at beginning of time step

δnN - Change in the number of moles of nitrogen

V_s - Volume of nitrogen supply

R - Universal gas constant, taken as 8.314 J/kg/K

T - Temperature, taken as 305 Kelvin

The density of nitrogen in the supply actuator and supply chamber of the cylinder also changes. These values were calculated using Equations 13 and 14 based on the change in nitrogen concentration in the supply chamber and supply actuator as well as the change in volume in the supply chamber.

In the nitrogen supply,

EQ. 13

$$\rho_{s,x+\delta x} = \frac{mM_n P_{s,x+\delta x}}{RT}$$

And in the chamber as,

EQ. 14

$$\rho_{ch,x+\delta x} = \frac{mM_n P_{ch,x+\delta x}}{RT}$$

The behavior of air on the compression side of the cylinder was also analyzed to determine the resistance to

cylinder motion developed by the compressed air. **Figure 11** illustrates the behavior of the cylinder on its compression side and the supply side

As the piston moves, the volume available within the cylinder decreases. This decrease is equal to $A_{cyl}\delta x$ and causes the pressure within the cylinder to increase. Initially, the air in the cylinder is at atmospheric pressure. However, due to the movement of the piston, the pressure increases along with the density of air. (Note: The duration of the event is so short that temperature change would have minimal effect.)

Considering a general position where the pressure is $P_{c,x}$ and density is $\rho_{c,x}$, the presence of the opening on the compression side of the cylinder will be assumed to function as an orifice with area A_{esc} and coefficient of discharge C_d. The nature of the gas flow was checked as either sub-critical, critical, or super-critical — and appropriate estimates of the escaping air velocity calculated using ISO Standard 4126-1, 2004. Using this methodology allows for an estimate of the mass flow rate of the air exiting the compression side of the cylinder. The pressure and density of the air on the compression side of the cylinder is estimated at the end of each time step as follows:

EQ. 15

$$P_{c,x+\delta x} = \frac{(n_{a,x} - \delta n_a)RT}{V_{c,x} - A_{cyl}\partial x}$$

EQ. 16

$$\rho_{c,x+\delta x} = \frac{mM_a P_{c,x+\delta x}}{RT}$$

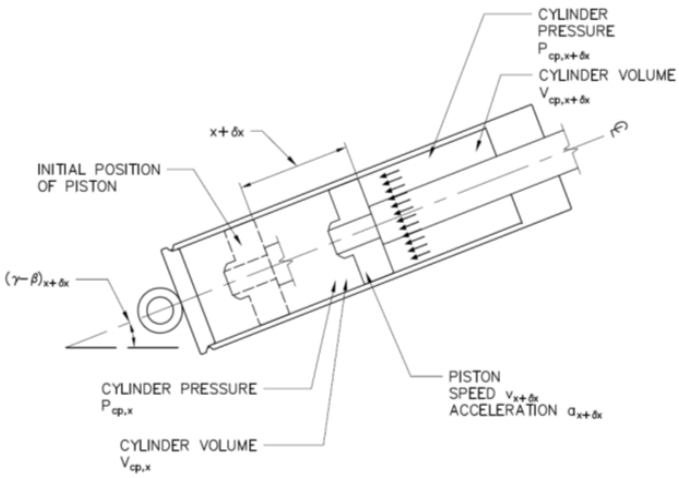

Figure 11
Pressure and volume on compression side of cylinder.

Where,

$P_{c,x+\delta x}$	-	pressure on compression side of cylinder at end of time step
$\rho_{c,x+\delta x}$	-	air density on compression side of cylinder at end of time step
$n_{a,x}$	-	number of moles of air in compression side of cylinder at start ot time step
δna	-	change in moles of air on compression side of cylinder over time step
mMa	-	Molecular mass of air, taken as 0.02891 kg/mol
A_{cyl}	-	area of cylinder

The resistance to the motion of the piston by the presence of air on the compression side of the cylinder can be estimated using the following expression:

$$F_{air,cyl} = C_{d,air}\frac{1}{2}A_{cyl}\rho_{c,x}v^2$$

The drag coefficient is assumed to be unity to maximize the effect of air resistance, reducing the above expression to:

EQ. 17

$$F_{air,cyl} = \frac{1}{2}A_{cyl}\rho_{c,x}v_x^2$$

Note: This variable was not measured in the cylinder and is considered to be small in comparison with the applied pressures.

Using the mathematical model of the geometry outlined in Equations 1 through 3, the reaction of the car's weight on the car flipper's arm and the resistance to the motion of the piston due to the car's weight, C_r can be calculated using Equations 4 and 5 for each position of the piston considered. Finally, the weight component of the piston acting to resist motion was considered as shown in Equation 18.

EQ. 18

$$W_p = m_p g \sin(\gamma - \beta)$$

Applying the Finite Difference Method

It is clear that the motion of the piston is continuous and that the velocity and acceleration can be determined by differentiation of the displacement time relationship. However, as the expressions derived to describe the geometry and forces on the piston do not allow for an analytical solution, the finite difference method replaces derivatives with discrete approximations[6]. In this regard, over a discrete time step, the change in velocity and displacement of the piston can be calculated.

The initial geometry of the car flipper and supply

actuator was known in addition to the dimensions of the cylinder. Starting at the initial conditions, the forces acting on the cylinder were calculated. Hence, the net force could be determined. The acceleration across the time step was calculated and the velocity and displacement estimated based on the calculated time step acceleration. The analysis relied on a forward pass method as only the initial conditions were known, and the accuracy of the results were limited to a first order analysis. In such an analysis, the error in the calculation was proportional to the time step chosen. For this reason, it was important to choose a very small time step that also satisfied convergence of results.

To determine the time step necessary to achieve this, several trials were run using varying time steps. To accommodate the numerous calculations required for the solution of the velocity-time relationship and to confirm convergence of the chosen time step, the analysis was coded using Visual Basic in the Microsoft Excel Environment. The velocity time relationship for various time steps using an actuator pressure of 3,000 psi is shown in **Figure 12**. As shown in this graphic, there is convergence of the results as the time step decreases — and at a time step of 0.0001 seconds, convergence is maximized.

The analysis was conducted for actuator pressures of 1,500 psi and 3,000 psi, the results of which are presented in **Figures 13** and **Figure 14**. As shown in these graphics, the velocity of the piston at the end of its stroke was approximately 14m/s under an actuator pressure of 1,500 psi and approximately 23m/s under an actuator pressure of 3,000 psi. Deceleration is due to the decrease in pressure on the supply side of the cylinder as the volume expands due to piston movement. Graphs of pressure on the supply side and compression side were added for the various actuator pressures.

Figures 15 and **16** show the pressure on the compression side of the cylinder for 1,500 psi and 3,000 psi actuator pressure.

Metallurgical Testing

The properties of the material from which the failed cylinder was fabricated was determined by destructive testing of the cylinder's material. Two samples were tested from which the yield strength and ultimate tensile strength were determined and compared with the grade of steel specified by the manufacturer (Grade 1020 CW, ASTM A519 Steel). The material was found to be consistent with

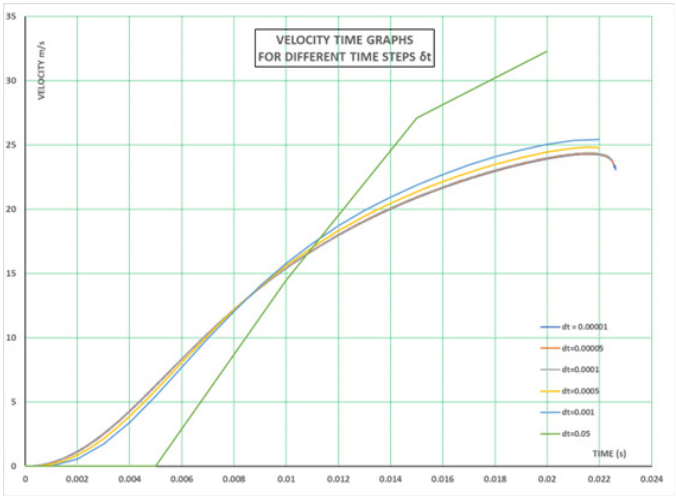

Figure 12
Velocity time relationship using various time steps and 3,000 psi actuator pressure.

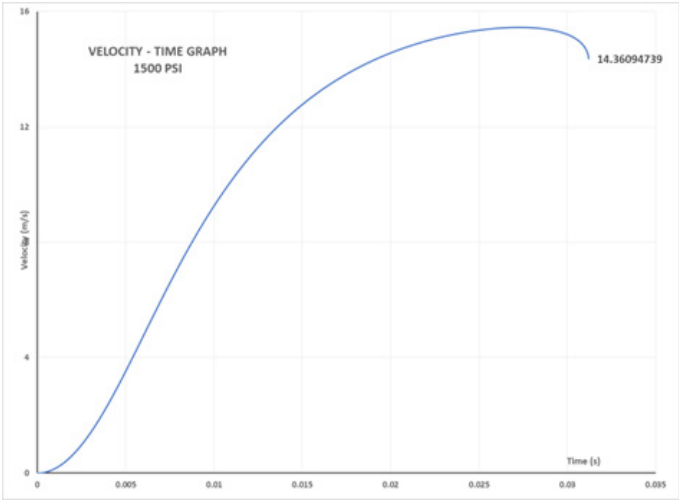

Figure 13
Velocity — time graph for 1,500 psi actuator pressure.

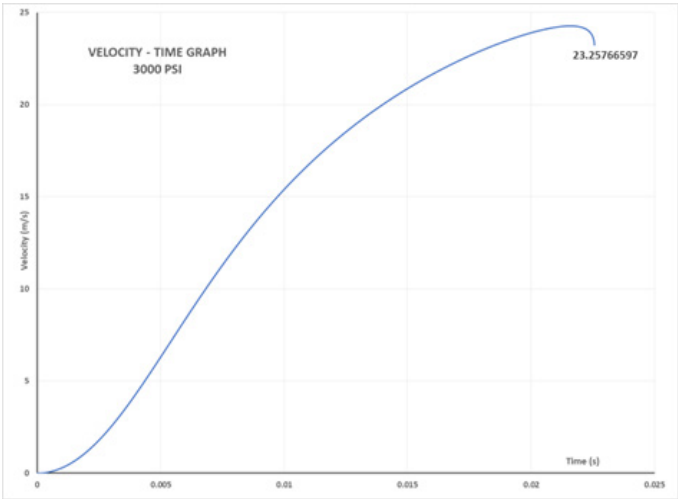

Figure 14
Velocity — time graph for 3,000 psi actuator pressure.

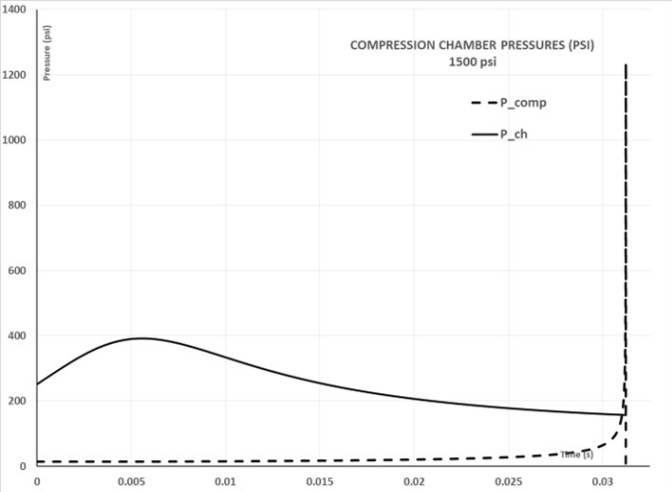

Figure 15
Compression and supply pressure in cylinder at 1,500 psi actuator pressure.

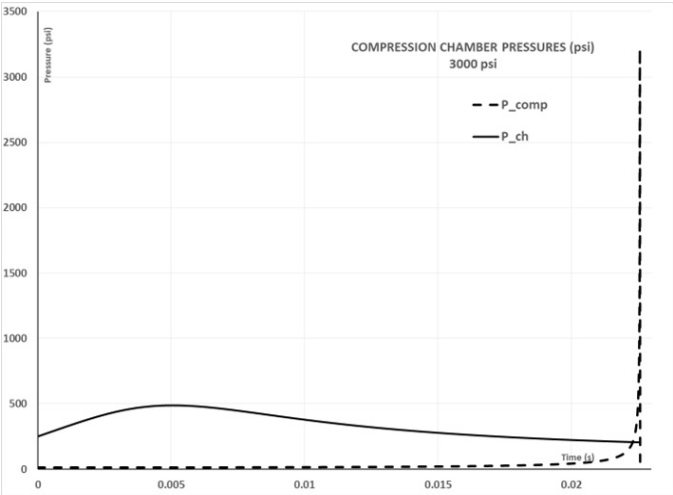

Figure 16
Compression and supply pressure in cylinder at 3,000 psi actuator pressure.

the grade of steel specified by the manufacturer.

Figure 17 shows a cross-section of the cylinder. The plane of fracture was located at the cylinder's end cap. The cylinder end cap was threaded onto the cylinder body, resulting in a smaller thickness than the cylinder wall. The equivalent spring method[7] was used to estimate the energy required for yielding and rupture of Member 2, taking into account the deformation in Member 1. Examinations of the piston did not reveal any significant deformation.

The stress-strain graphs of the cylinder material was obtained from testing and used in conjunction with the equivalent spring method to calculate the amount of energy required to cause rupture. The stress-strain curves are

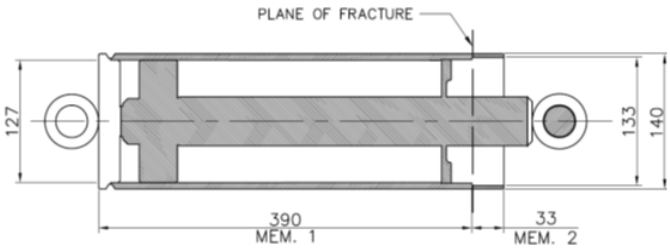

Figure 17
Cross-section of cylinder showing member identification.

shown in **Figure 18**.

The expression developed for this calculation is shown below:

$$E = Al\int_0^{\varepsilon} \sigma\,\delta\varepsilon \qquad \text{EQ. 19}$$

Where,

E	-	Rupture energy
A	-	Cross-sectional area of member
l	-	length of member
$\int_0^{\varepsilon} \sigma\,\delta\varepsilon$	-	area under stress-strain graph

The cylinder was analyzed as two discrete sections: the thicker body (wall thickness of 6.5 mm) and the thinner end cap (wall thickness 3.5 mm) connected in series. Two samples were tested to obtain the stress-strain graph. It was found that the energy required for rupture of the

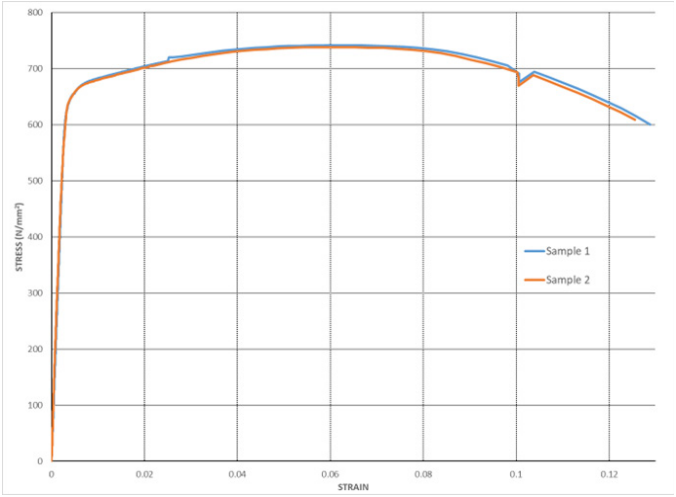

Figure 18
Stress-strain graphs from testing.

thinner end cap was between 4500 Nm to 7000 Nm. For this reason, the impact force was considered to be the same in each member, but the stresses differed due to wall thickness, as did the strain.

The limiting force is the rupture force in the thinner member, which was calculated using the ultimate stress from testing and found to be approximately 1100kN. The stress in the thicker member at this force was found to be below the material's yield stress, and the stress-strain relationship was linear. The energy absorbed by the thicker member, determined using Equation 19, was found to be approximately 360Nm. Thus, the total energy required to be imparted into the cylinder from impact ranged between 4860Nm and 7360Nm and was the minimum kinetic energy required by the piston for rupture. The piston velocity for this to occur was estimated to be 37.1m/s. This analysis was also done for yielding, and the speed required was found to be 8m/s.

Referring to **Figure 13** and **Figure 14**, the velocity at the end of the piston's stroke was approximately 14m/s under an actuator pressure of 1,500 psi and approximately 23m/s under an actuator pressure of 3,000 psi. These velocities were less than the 37 m/s required to result in rupture but greater than the 8m/s required to result in yielding. Therefore, yielding likely occurred in Member 2 on the first trial run at 1,500 psi. The further application of an actuator pressure of 3,000 psi likely resulted in further permanent deformation of the cylinder. The final application of 3,000 psi actuator pressure would have been adequate to result in rupture of the cylinder adjacent to the threaded section holding the cap in place, due to the continued plastic deformation on previous trials.

The results of the SEM examination and impact testing (laboratory tests on samples using Charpy V-notch tests per ASTM E23-18 in the longitudinal direction of the cylinder cap) supported the preceding discussion. As shown in **Figure 19**, significant portions of the fracture surface showed cleavage facets that indicated a brittle process[8]. This loss of ductility was likely due to high strain rates associated with impact load.

The examination was done on the fracture surface of the end cap. The orientation of the end cap was on the annulus of the wall thickness. Impact tests conducted at samples near the fracture surface in the longitudinal direction returned results (ranging between 3 to 5 Joules) that were approximately 80% of expected values for carbon steel at 20°C[9]. Failure occurred when stresses were repeatedly between yield and ultimate. Impact testing showed 20% of expected value. Referencing **Figure 19**, impact loading was investigated by considering the minimum velocity required to develop the kinetic energy required for yielding and rupture. Brittle failure occurred because the initial operation of the car flipper was such that the kinetic energy was more than enough to cause yielding, but not rupture. Each time the device was run, the end cap plastically deformed until its ability to absorb further impact was so diminished that rupture occurred below ultimate stress values.

There was also some evidence of accompanying ductile fracture near the inner and outer diameters of the end cap, as shown in **Figure 20**. There was no evidence of striations, beach marks, or corrosion damage observed in the SEM examination.

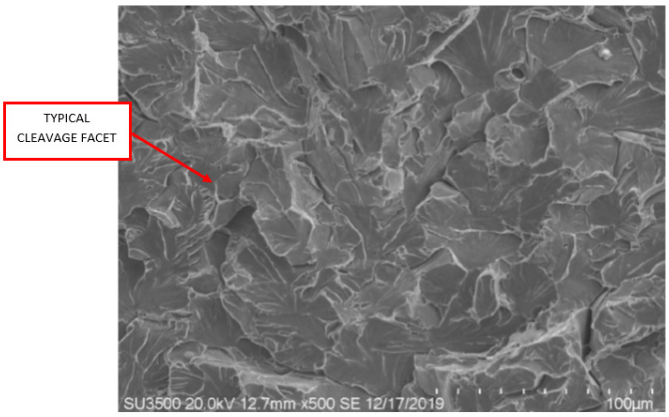

Figure 19
Cleavage facets on majority of fracture surface.

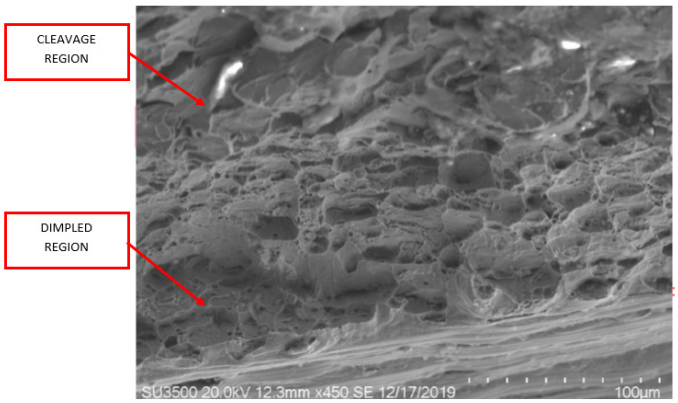

Figure 20
Dimpling near inner diameter.

Review of Manufacturer's Specifications

The manufacturer of the cylinder was contacted regarding the general suitability of the cylinder to the function in the car flipper application. The manufacturer confirmed that the cylinder was intended to be used in a double acting application using hydraulic oil over a working range of 0 to 3,000 psi. The manufacturer further confirmed that the allowable piston speed is 0.168 m/s, and — if used in a pneumatic application — the working pressures reduce to 87 to 116 psi. Therefore, the use of the cylinder in a single-acting application using compressed nitrogen at 3,000 psi was outside the manufacturer's specifications. Furthermore, the velocity of the piston exceeded manufacturer's specifications.

Conclusions

- The cylinder was not used in a double-acting application and utilized compressed nitrogen at pressures far greater than the manufacturer's specifications.
- The finite difference analysis demonstrated that the likely piston speed exceeded the manufacturer's specifications.
- The velocity of the piston ranged between 14 m/s at a supply pressure 1,500 psi (10.3 MPa) and 23 m/s at a supply pressure of 3,000 psi (20.6 MPa).
- The movement of the piston and rod was arrested at the end of the piston's stroke by impact with the cylinder. The piston was stopped by impact with the end cap.
- In the area of impact between the piston and the cylinder, the cylinder's wall thickness was reduced to accommodate threads for the securement of the cylinder's end cap. The fracture surface occurred in this area of reduced wall thickness in the cylinder.
- The range of speeds of the piston exceeded the ability of the cylinder to absorb the impact energy without yielding.
- The continued use of the car flipper at an actuator pressure of 1,500 psi (10.3 MPa) followed by an additional attempt at an actuator pressure of 3,000 psi (20.6 MPa) successively reduced the ability of the cylinder to absorb the energy of the impacts.
- On the final operation of the car flipper, at an actuator pressure of 3,000 psi (10.3 MPa), the cylinder could no longer absorb the kinetic energy of the piston/rod, and rupture of the cylinder occurred.

References

1. J. McCarthy, An Introduction to Theoretical Kinematics, Cambridge: MIT Press, 1990, p. Chapter 1.
2. Crane, Flow of Fluids Technical Paper 410M, New York: Crane Company, 1982, p. Chapter 1.
3. M. R. Lindeburg, PE Civil Reference Manual, Sixteenth Edition, Belmont: Professional Publications Inc., 2018, p. Chapter 17.
4. S. C. R. Chapra, Numerical Methods for Engineers, Sixth Edition, New York: McGraw-Hill Companies Inc., 2010, p. Chapter 6.
5. R. Mortimer, Physical Chemistry Third Edition, London: Elsevier Academic Press, 2008, p. Chapter 1.
6. R. LeVeque, Finite Difference Methods for Ordinary and Partial Differential Equations, Seattle: Society of Industrial and Applied Mathematics, 2007, p. Chapter 1.
7. R. Hibbler, Mechanics of Materials, 6th Edition, New Jersey: Prentice Hall, 2004, p. Chapter 14.
8. A. Liu, Mechanics and Mechanisms of Failure: An Introduction, Ohio: ASM International, 2005, p. Chapter 2.
9. ASM International, Steel Castings Handbook, 6th Edition, ASM International, 1995, p. Chapter 23.
10. ISO, Safety devices for protection against excessive pressure Part 1 - Safety Valves, ISO, 2004, p. Chapter 8.